Novel Kinetic and Background Current Selectivity in the Even Harmonic Components of Fourier Transformed Square-Wave Voltammograms of Surface-Confined Azurin

Jie Zhang,[†] Si-Xuan Guo,[†] Alan M. Bond,*[,†] Michael J. Honeychurch,[†,‡] and Keith B. Oldham[§]

School of Chemistry, Monash University, Clayton, Victoria 3800, Australia, and Department of Chemistry, Trent University, Peterborough, Ontario, Canada K9J 7B8

Received: November 25, 2004

Fourier transform analysis of ramped square-wave voltammograms indicates the availability of a novel form of kinetic selectivity for surface-confined electron-transfer processes. Thus, for all the even harmonic components, quasi-reversible processes are sensitive to the surface coverage, the reversible potential, the electron-transfer rate constant ($k^{0'}$), and the electron-transfer coefficient (α), as well as to the amplitude (ΔE) and frequency (f) of the square wave and dc scan rate. Additionally, it is insensitive to background capacitance current. In contrast, reversible processes and background currents are predicted to be absent from the even harmonics and only detectable in the odd harmonic components. The square-wave voltammetry of the surface-confined quasi-reversible azurin process azurin[Cu(II)] + $e^- \rightleftarrows$ azurin[Cu(I)] at a paraffin-impregnated graphite electrode has been employed as a model system to test theoretical predictions. Most voltammetric characteristics of the even harmonic components obtained from the Fourier analysis are consistent with electrode kinetic values of $k^{0'} = 90\ s^{-1}$ and $\alpha = 0.48$, although some nonideality possibly due to kinetic dispersion also is apparent. Conditions also have been determined under which a readily generated waveform constructed from the Fourier series of sine waves produces voltammograms that are essentially indistinguishable from those predicted when an ideal square wave is employed.

1. Introduction

Currently, there is considerable interest in the electrochemistry of surface-confined electron-transfer processes[1−4] that are important in problems of biological[2,4] and fundamental interest.[1,3] Direct current (dc) techniques, in linear (staircase) or cyclic modes, are the most common forms of voltammetry used in these studies.[1−3] A significant advantage in using dc techniques is the widespread availability of theory for many mechanisms.[5] However, quantitative analysis of experimental data requires the use of a wide range of scan rates. This presents difficulties, as many experiments may be required to be undertaken with unstable electroactive films. Furthermore, in the case of high-molecular-weight surface-attached proteins and enzymes, extraction of the required Faradaic current is difficult, because background current commonly dominates the measured total current.[2a]

Square-wave voltammograms, analyzed in the time domain,[6] have been employed in studies of surface-confined species[7] in order to minimize problems with background current. For diffusing systems, the contribution of the background current can be significantly suppressed by careful choice of the current sampling protocol, because the decay of the charging current occurs at a faster rate than for Faradaic current.[6] The time dependence of Faradaic to charging current ratio is more complex for diffusionless surface-confined systems, so the advantage of the square-wave method for this class of mechanism is not so obvious.

Recently, the analysis of square-wave voltammetry has been reported in the frequency rather than the time domain for diffusion-based processes.[8,9] In the version of the technique employed, the square wave is superimposed on a linear dc ramp to provide a waveform (Figure 1) which is similar to that employed in Barker square-wave voltammetry.[10] However, it differs from the more widely used Osteryoung approach, where the square wave is superimposed onto a staircase voltage.[11]

In the present study, the analysis of square-wave linear sweep voltammetry for surface-bound species is developed in the frequency domain with the aim of assessing if significant advantages compared with the traditional forms of the technique can be achieved with respect to kinetic sensitivity, improved Faradaic-to-background current ratio, and experimental efficiency. The approach utilizes Fourier analysis to separate the data into the dc component and the constituent ac harmonics. Significantly, the response for all the even harmonics is predicted to be insensitive to charging current and only sensitive to quasi-reversible and not reversible processes. This outcome represents a novel form of both background and Faradaic selectivity.

A square wave is equivalent to a specific combination of sine waves of frequencies that are odd multiples of the square wave's frequency as shown in eq 1

$$(-)^{\mathrm{int}(\omega t/\pi)}\Delta E = \frac{4\Delta E}{\pi}\sum_{n=1}^{K}\frac{\sin[(2n-1)\omega t]}{2n-1} \quad \text{with } K=\infty \tag{1}$$

where ω is the angular frequency, ΔE is the amplitude of the square wave, and t is time. A theoretical study has been undertaken to define the conditions under which results obtained with the readily implemented multisine-wave (K is a large integer) version is experimentally indistinguishable from that

* E-mail: Alan.Bond@sci.monash.edu.au.
[†] Monash University.
[‡] Present address: Department of Chemistry, School of Molecular and Microbial Sciences, University of Queensland, St. Lucia 4072, Queensland, Australia.
[§] Trent University.

10.1021/jp044614s CCC: $30.25
Published on Web 04/14/2005

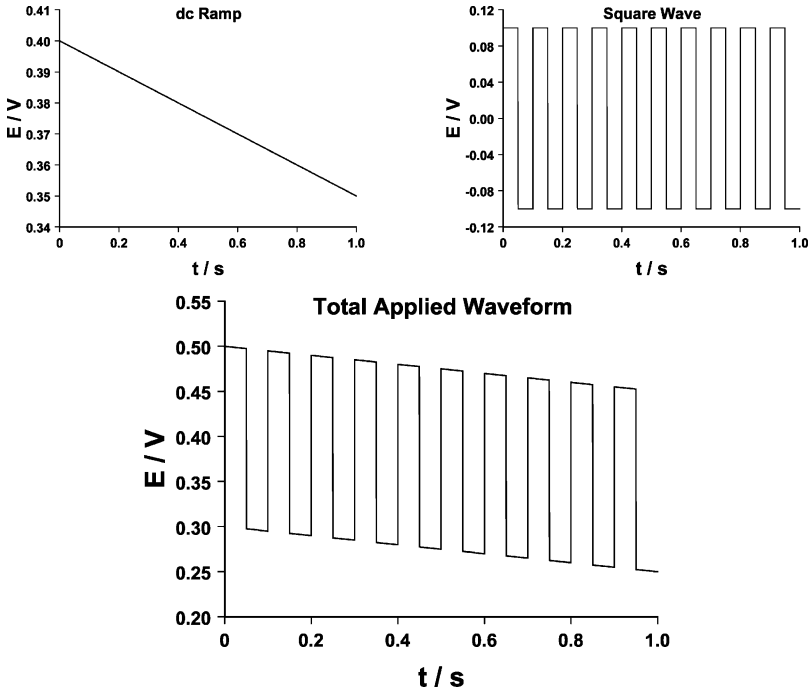

Figure 1. Waveform employed in square-wave voltammetric measurements (initial reduction sweep direction only shown).

of a square wave. The advantage of the multisine waveform approach is that it avoids experimental (e.g., infinite current) problems arising from the discontinuity of a true square wave.

Theoretical predictions have been tested using the reduction of surface-bound azurin. Armstrong and co-workers[2a,7a,12] have shown that surface-confined thin-film voltammetry of this copper-containing metalloprotein almost provides a model system. Data analyzed by dc,[12] square-wave (time domain),[7a] and sinusoidal-wave[13] methods are available for comparison.

2. Experimental Section

2.1. Chemicals. *Pseudomonas aeruginosa* azurin, a protein of molecular weight 14 125 Da,[14] was extracted and purified according to the literature.[15] The protein solution, azurin (3.0 mg mL^{-1}) in HEPES buffer (20 mM, pH 7.0), was stored in the dark at 4 °C.

A buffer solution (pH 8.0) containing 0.02 M tris(hydroxymethyl)methylamine [$(HOCH_2)_3CNH_2$, 99%] (Aldrich Chemical Co., Milwaukee, WI) and 0.1 M NaCl (BDH Laboratory Supplies, Poole, U.K., AnalaR) was used in the voltammetric measurements. The pH value was adjusted using an aqueous NaOH (BDH, AnalaR) or HCl (32%, BDH, AnalaR) solution and was measured with a Metrohm 744 pH meter, equipped with a Metrohm pH glass electrode (Metrohm Ltd., Herisau, Switzerland). The pH value of 8.0 was chosen to avoid the complication associated with acid−base reactions being coupled to the electron-transfer process.[12b] All reagents were used as received. All solutions were prepared using water (resistivity 18 MΩ cm) purified with a MilliQ water purification system (Millipore Corp., Massachusetts, U.S.A.).

2.2. Apparatus and Procedures. Full details of the instrumentation used in the square-wave voltammetric measurements are available elsewhere.[16] The experiments are arranged so that exactly 2^m (typically, $m = 15$ or 16) points (convenient for Fourier analysis) of $I-t$ data are collected at a constant sampling rate of about 40 kHz. This restricts the highest frequency to be analyzed to 20 kHz according to Nyquist'ssampling theorem.[17] A specified number of sine waves in the Fourier series representation given in eq 1 were used to generate the required waveform. If the first 20 (or more) odd multiples of the square wave's frequency terms were used, then the applied waveform employed can be regarded as experimentally equivalent to a square wave within experimental error (see Section 3.4.2). The dc and harmonic components were separated by Fourier analysis in the usual manner.[13]

A conventional three-electrode cell was employed in all electrochemical measurements, with Ag/AgCl (saturated KCl) as the reference electrode, platinum wire as the auxiliary electrode, and a paraffin-impregnated graphite rod (PIGE, radius 3 mm)[18−20] working electrode.

The procedure for the fabrication of a protein film electrode has been described in detail elsewhere.[2a,7a,12,14] In summary, prior to the protein film deposition, the PIGE electrode was polished with 0.3-μm alumina on a clean polishing cloth (Buehler), rinsed with water, and then sonicated in water to remove alumina. The electrode was then placed in ice with the surface pointed upward until it was ice-cold. Next, a 2−5-μL drop of azurin solution was placed onto the cold upturned electrode surface. The azurin-adsorbed electrode was then immediately transferred into the standard three-electrode cell containing a buffer solution, which had been purged with nitrogen for at least 15 min and cooled to 0 °C with a water/ice bath. Azurin film electrodes prepared by this procedure are stable for several hours.

The experimental studies were undertaken in a highly conducting aqueous electrolyte solution (0.1 M NaCl). Because the surface concentration of azurin is low (only about 10^{-11} mol cm^{-2}), and consequently, currents measured are also low, the effect of uncompensated resistance of ca. 30 Ω has been neglected. Problems with a variable interfacial potential distribution[21] that arise when a surface-bound compact monolayer (no ion penetration into the layer) is present also were neglected. In the case of an adsorbed monolayer of the large and flexible azurin molecule, there are likely to be gaps available for the

small supporting electrolyte ions to approach the electrode surface and hence avoid this difficulty.

All voltammetric measurements were carried out at 0 °C.

3. Theoretical Analysis of Square-Wave Voltammetry for a Surface-Confined Process

3.1. General Principles. The basic principles of the theory of square-wave voltammetry of surface-confined species in the frequency domain are the same as described for sine-wave ac voltammetry.[13,22] Thus, we will consider a one-electron-transfer reduction process

$$\mathrm{O(surf)} + \mathrm{e}^- \underset{k_b}{\overset{k_f}{\rightleftharpoons}} \mathrm{R(surf)} \tag{2}$$

where O and R are the surface-confined oxidized and reduced species, respectively (charge omitted for simplicity), and k_f and k_b are the forward and backward electron-transfer rate constants, respectively. If the potential dependence of the rate constants is assumed to obey the Butler−Volmer formalism,[6] instead of the more complicated Marcus theory,[23,24] then

$$k_f = k^{0'} \exp\left[\frac{-\alpha F}{RT}(E - E^{0'})\right] \quad \text{and } k_b = k^{0'} \exp\left[\frac{(1-\alpha)F}{RT}(E - E^{0'})\right] \tag{3}$$

where $k^{0'}$ is the formal electron-transfer rate constant at $E^{0'}$, the formal potential of the redox couple; α is the electron-transfer coefficient; E is the applied potential at time t; and R, T, and F have their usual meanings. If it is assumed that O and R are both surface-confined or strongly adsorbed on the electrode surface and the adsorption follows a Langmuir isotherm, then the Faradaic current, I, is given by

$$I = FA\Gamma[k_b(1-\theta) - k_f\theta] \tag{4}$$

where A is the area of the electrode, Γ is the total surface concentration of the bound electroactive species (oxidized and reduced forms), and θ is the potential dependent surface coverage of the oxidized form. Equation 4 assumes lateral molecular interactions, and heterogeneity of the layer, can be ignored,

The potential at time t in ramped square-wave voltammetry is given by eq 5 for a reduction process

$$E(t) = E_{dc}(t) + E_{ac}(t) = E_{start} - \upsilon t + E_{ac}(t) \tag{5}$$

where υ is the scan rate of the dc ramp and E_{start} is the starting or initial value of the potential.

Two types of ac waveforms are considered. The first is a true square wave of angular frequency ω and amplitude ΔE which may be represented either by the integer−value function formulation or as an infinite sum of sine waves of frequencies that are odd multiplies of ω.

$$(E_{ac})_{sw} = (-)^{\mathrm{int}(\omega t/\pi)}\Delta E = \frac{4\Delta E}{\pi}\sum_{n=1}^{\infty}\frac{\sin[(2n-1)\omega t]}{2n-1} \tag{6}$$

The second, which is used experimentally in studies on azurin for practical reasons, is defined by the equation

$$(E_{ac})_{ms} = \frac{4\Delta E}{\pi}\sum_{n=1}^{K}\frac{\sin[(2n-1)\omega t]}{2n-1} \tag{7}$$

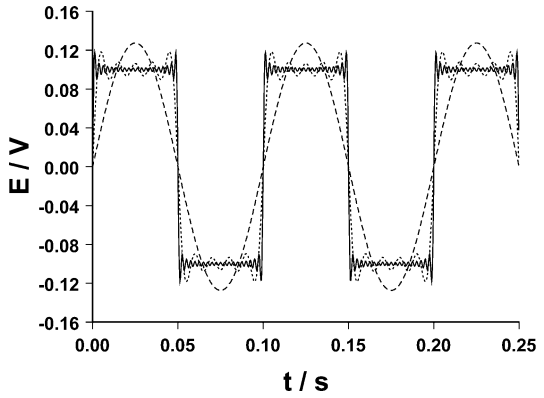

Figure 2. The waveform generated using the sum of a series of sine waves as described by eq 7 with $K = 1$ (- - -), 5 (·····), and 20 (—).

This multisine-wave approach differs from a square wave in that the sine components of angular frequencies higher than $(2K - 1)\omega$ are omitted. Figure 2 shows that when K becomes sufficiently large ($K \geq 20$), an excellent approximation of a square-wave signal is generated, but without having to introduce a discontinuity. Clearly, while mathematically describable, a perfect square wave cannot be generated experimentally. In contrast, eq 7 is readily implemented experimentally.

3.2. Analytical Solution for a Reversible Process. For a reversible process involving bound species O(surf) and R(surf), the Bulter−Volmer formalism can be replaced by the Nernst equation

$$E(t) = E^{0'} + \frac{RT}{F}\ln\left[\frac{\Gamma_{ox}}{\Gamma_{red}}\right] \tag{8}$$

where Γ_{ox} and Γ_{red} are the surface concentrations of the surface-confined oxidized and reduced electroactive species, respectively. Thus

$$\frac{\Gamma_{ox}}{\Gamma_{red}} = \frac{\Gamma_{ox}}{\Gamma - \Gamma_{ox}} = \frac{\theta}{1-\theta} = \exp\left\{\frac{F}{RT}[E(t) - E^{0'}]\right\} \tag{9}$$

Equation 9 may be rearranged to

$$\theta = \frac{\exp\{F[E(t) - E^{0'}]/(RT)\}}{1 + \exp\{F[E(t) - E^{0'}]/(RT)\}} = \frac{1}{2}\left[1 + \tanh\left\{\frac{F}{2RT}[E(t) - E^{0'}]\right\}\right] \tag{10}$$

To combine this expression with eqs 5 and 6, it is convenient to introduce the terms ξ_{dc} and $\Delta\xi$, so that

$$\frac{F[E(t) - E^{0'}]}{2RT} = \frac{F}{2RT}(E_{start} - E^{0'} - \upsilon t) + (-)^{\mathrm{int}(\omega t/\pi)}\frac{F\Delta E}{2RT} = \xi_{dc} + (-)^{\mathrm{int}(\omega t/\pi)}\Delta\xi \tag{11}$$

It therefore follows from eqs 10 and 11 that

$$\begin{aligned} 2\theta - 1 &= \tanh\{\xi_{dc} + (-)^{\mathrm{int}(\omega t/\pi)}\Delta\xi\} \\ &= \frac{1}{2}[\tanh(\xi_{dc} + \Delta\xi) + \tanh(\xi_{dc} - \Delta\xi)] + \\ &\quad \frac{1}{2}(-)^{\mathrm{int}(\omega t/\pi)}[\tanh(\xi_{dc} + \Delta\xi) - \tanh(\xi_{dc} - \Delta\xi)] \end{aligned} \tag{12}$$

The final step required to generate eq 12 is validated in an appendix contained in ref 25.

According to eq 13

$$I = FA\Gamma \frac{d\theta}{dt} \tag{13}$$

In order to obtain the current, it will be necessary to differentiate eq 12 with respect to time. In anticipation of the need for this step, note that

$$\frac{d}{dt}\xi_{dc} = \frac{-F\nu}{2RT} \tag{14}$$

$$\frac{d}{dt}[(-1)^{\text{int}(\omega t/\pi)}] = \frac{4\omega}{\pi}\sum_{n=1}^{\infty}\cos[(2n-1)\omega t] \tag{15}$$

The hyperbolic tangent terms in eq 12 generate squared hyperbolic secants on differentiation and thus give rise to terms that we denote as follows:

$$S_+ = \text{sech}^2(\xi_{dc} + \Delta\xi) \text{ and } S_- = \text{sech}^2(\xi_{dc} - \Delta\xi) \tag{16}$$

For computational purposes, these terms are readily calculated in their exponential forms

$$S_\pm = \text{sech}^2(\xi_{dc} \pm \Delta\xi) = \frac{4\exp[2(\xi_{dc} \pm \Delta\xi)]}{\{1+\exp[2(\xi_{dc} \pm \Delta\xi)]\}^2} \tag{17}$$

Bearing these preliminary outcomes in mind, differentiation of eq 12 leads to

$$\frac{d\theta}{dt} = -\frac{F\nu}{8RT}(S_+ + S_-) - (-)^{\text{int}(\omega t/\pi)}\frac{F\nu}{8RT}(S_+ - S_-) + \frac{\omega}{\pi}[\tanh(\xi_{dc} + \Delta\xi) - \tanh(\xi_{dc} - \Delta\xi)]\sum_{n=1}^{\infty}\cos[(2n-1)\omega t] \tag{18}$$

Combination of eq 18 with eq 13 gives

$$I_{dc} = -\frac{F^2 A\nu\Gamma}{8RT}(S_+ + S_-) \tag{19}$$

and

$$I_{ac} = -\frac{F^2 A\nu\Gamma}{2\pi RT}(S_+ - S_-)\sum_{n=1}^{\infty}\frac{\sin[(2n-1)\omega t]}{2n-1} + \frac{\omega FA\Gamma}{\pi}[\tanh(\xi_{dc} + \Delta\xi) - \tanh(\xi_{dc} - \Delta\xi)]\sum_{n=1}^{\infty}\cos[(2n-1)\omega t] \tag{20}$$

As shown in Figure 3, the implications of eq 19 are clear. The dc component of a reversible Faradic response to a square-wave perturbation for a surface-confined process is predicted to be the average of two pure dc voltammograms, one shifted to positive potentials by ΔE and the other shifted to negative potentials by $-\Delta E$. This outcome is consistent with the finding of others[7f,26] for surface-confined processes and also is observed in the case of a Nerstian process for dissolved species.[8,25] As required, a dimensionless dc current, $I_{DC,NORM}$ (vide infra notes 28d for definition), of -0.25 is obtained at the peak potential when $\Delta E = 0$, because this situation corresponds to that expected for a reversible linear sweep voltammogram for a surface-confined process.[6]

The results in eq 20 suggest that there are no even harmonic components from the ramped square-wave voltammetry of a reversible process, as is also the case when electroactive species

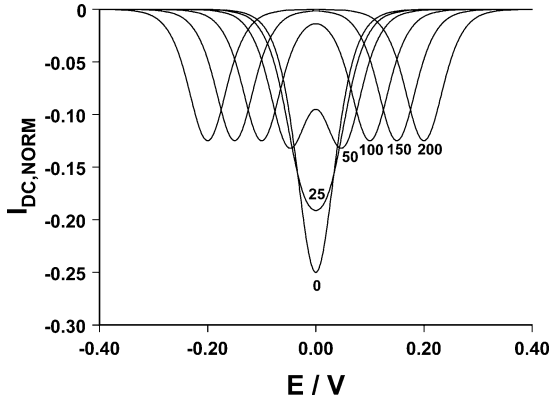

Figure 3. Dependence of the dc component of a reversible surface-confined square-wave voltammogram on ΔE (0−200 mV as indicated). Voltammograms calculated according eq 19 with $f = 10$ Hz, $\nu = 50$ mV s^{-1}, and other parameters defined in the text.

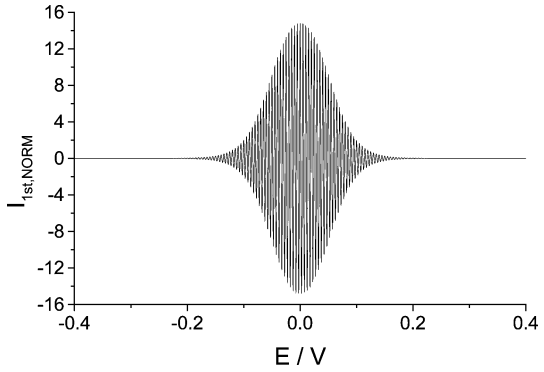

Figure 4. First harmonic component for a reversible surface-confined process calculated according to eq 20 with $f = 10$ Hz, $\Delta E = 50$ mV, $\nu = 50$ mV s^{-1}, $C_{dl} = 0$, and other parameters defined in the text.

are dissolved in the solution phase.[25] The first harmonic ac component (i.e., the fundamental component, corresponding to $n = 1$), calculated by eq 20 for a reversible surface-confined process in the absence of double layer charging, is shown in Figure 4. All characteristics of the higher odd harmonic components, including the envelope shape and peak height, are very similar to those shown for the first harmonic component.

The contribution of the double layer charging current, I_{dl}, to the total current can be calculated, assuming C_{dl} is independent of potential, from the relationship

$$I_{dl} = C_{dl}\frac{dE}{dt} \tag{21}$$

Thus, from eqs 5 and 6

$$I_{dl} = C_{dl}\left\{-\nu + \frac{4\omega\Delta E}{\pi}\sum_{n=1}^{\infty}\cos[(2n-1)\omega t]\right\} \tag{22}$$

Equation 22 predicts that all the odd harmonic charging current components have the same frequency as the applied sine-wave series and have an amplitude of $4\omega\Delta EC_{dl}/\pi$ and also that no even harmonic contributions will be present. The latter observation is extremely important, as it implies that, if the Faradaic process generates even harmonics (as is the case for a quasi-reversible process), then measurements of these components will provide exceptionally favorable Faradaic-to-charging current ratios.

3.3. Numerical Simulation. Equations 4, 5, 6 (or 7), and 13 can be combined and solved to give an expression for the

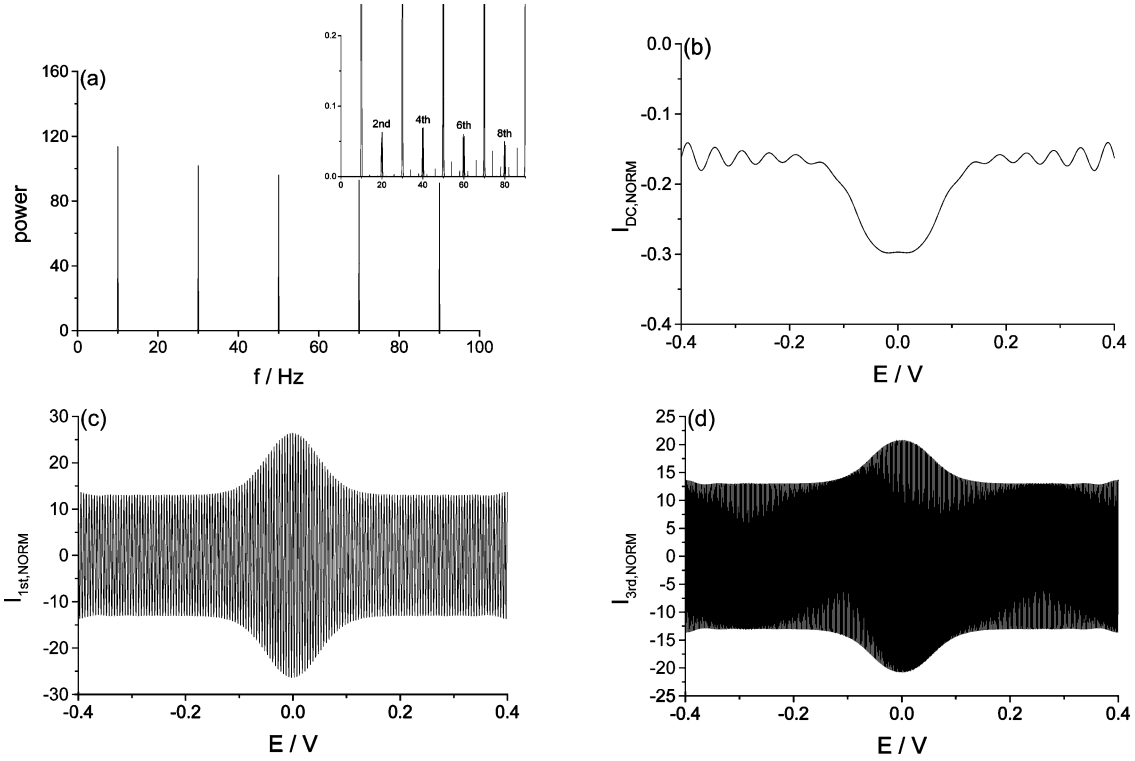

Figure 5. Power spectrum (a), dc (b), and odd harmonic (c, first; d, third) components deduced by Fourier analysis of a simulated quasi-reversible process with $k^{0'} = 50\ s^{-1}$, $\alpha = 0.5$, $f = 10$ Hz, $E^{0'} = 0$, $\Delta E = 50$ mV, $\upsilon = 50$ mV s^{-1}, and $C_{dl} = 0.2$ F m^{-2}.

current−time relationship for a quasi-reversible process. Unfortunately, unlike the situation prevailing for the reversible case, no analytical solution is available. Consequently, numerical simulations, as almost universally adopted in dc voltammetric studies of quasi-reversible surface-confined processes,[1,7] are required to predict the theoretical behavior expected for the square-wave case.

The general procedure used in numerical simulations of a surface-confined process is to replace the continuous ramp by a waveform that contains a series of very small potential increments (sufficiently small so that the calculated current is independent of the size of the potential increment). During the course of the simulation, the potential within each individual potential increment is assumed to be constant, and both the potential and the potential-dependent surface coverage are updated at the end of each potential increment. An average current is calculated on the basis of the change of the surface concentrations of electroactive species for each small potential increment. The reader is referred to refs 7g and 27 for further details of the numerical simulation of a surface-confined process. In the present simulation of a square-wave voltammogram, a minimum of 150 potential increments (corresponding to a potential increment of about 0.01 mV) was used to define each half of the square-wave period (see Figure 1). Because the potential is constant, both k_f and k_b also can be considered to be constant for the duration of the increment. The combination of eqs 4 and 13 produces the differential equation

$$\frac{d\theta}{dt} = k_b - (k_f + k_b)\theta \tag{23}$$

which, in principle, could serve as the basis of the simulation by continually updating the coverage by the formula

$$\theta(t + \delta t) = \theta(t) + [k_b - (k_f + k_b)\theta(t)]\delta t \tag{24}$$

However, in practice, this process behaves poorly unless unrealistically small values of t are used. As an alternative, we adopted a procedure based on the integration of eq 23 to

$$\ln[k_b - (k_f + k_b)\theta] = -(k_f + k_b)t + C_1 \tag{25}$$

followed by exponentiation to give

$$k_b - (k_f + k_b)\theta = C_2 \exp[-(k_f + k_b)t] \tag{26}$$

where C_1 and C_2 are constants. Because we assume that the rate constants do not change in the brief interval t, during which θ increases by $\delta\theta$, we can also write

$$k_b - (k_f + k_b)(\theta + \delta\theta) = C_2 \exp[-(k_f + k_b)(t + \delta t)] \tag{27}$$

Subtraction of the last two equations produces

$$(k_f + k_b)\delta\theta = C_2 \exp[-(k_f + k_b)t][1 - \exp[-(k_f + k_b)\delta t)] \tag{28}$$

which, after substitution from eq 26 to eliminate C_2, leads to the result

$$\theta(t + \delta t) = \theta + \delta\theta = \theta + \left(\frac{k_b}{k_f + k_b} - \theta\right)\{1 - \exp[-(k_f + k_b)\delta t]\} \tag{29}$$

This is the vehicle by which the coverage was continually updated in our simulation. Equation 29 is preferable to eq 24, because the former is not based on a formula that regards δt as infinitesimal. The current was then calculated from

$$\frac{I}{FA\Gamma} = \frac{\delta\theta}{\delta t} = \left(\frac{k_b}{k_f + k_b} - \theta\right)\frac{\{1 - \exp[-(k_f + k_b)\delta t]\}}{\delta t} \tag{30}$$

For the purpose of solving eq 30 numerically, it is useful to introduce the dimensionless variables given in the notes.[28] In this way, the expression for the dimensionless current, I_{norm}, can be obtained

$$I_{norm} = \frac{\delta\theta}{\delta\tau} = \frac{[K_b/(K_f + K_b) - \theta]\{1 - \exp[-(K_f + K_b)\delta\tau]\}}{\delta\tau} \quad (31)$$

Equation 31 can be solved numerically by the finite difference method to give the total Faradaic current as a function of time (or potential) and the dc and ac harmonic components obtained by use of Fourier analysis in the normal way.[13] The procedure gives a numerically stable solution for all rate constants and hence can be used to simulate reversible, quasi-reversible, and irreversible processes. The normalized charging current can be obtained on the basis of eq 21 and the relationships in the notes[28b,d,i] and added, when necessary, to the Faradaic current. Fortran programs for Fourier analysis of surface-confined square-wave voltammograms are available on request to the authors.

3.4. Discussion of Results of Numerical Simulations. *3.4.1. The Case Where the Square Wave Is Generated Using Eq 6.* Numerical simulations enable the influences of f, ΔE, $k^{0\prime}$, and α in ramped square-wave voltammetry to be established for a quasi-reversible surface-confined process. In particular, we are interested in understanding the response of the dc and ac (even and odd) harmonics, for the Faradaic and charging processes. Equation 6 was employed to generate a square wave in the initial theoretical analysis of a quasi-reversible surface-confined process. For discussion purposes, the parameter $E^{0\prime} = 0$, starting potential = 0.4 V, and end potential = −0.4 V are assumed, and voltammetric data are presented in a dimensionless form, which means that the normalized Faradaic current is independent of Γ, T, and A, in accordance with the relationship in the notes.[28d]

3.4.1.1. DC and Odd Harmonic Components. As required, the numerical simulations and the analytical equations give the same result ($<1 \times 10^{-3}$% difference in the peak current) when Fourier analysis is used to obtain the dc and odd harmonic components for a reversible process. The numerical simulation of a reversible process was undertaken using the theory for a quasi-reversible process with a very large $k^{0\prime}$ value of 1×10^8 s^{-1}.

Figure 5 contains the power spectrum,[17] as well as Fourier analysis deconvolved dc and odd harmonic (first and third) components of a simulated voltammogram for a quasi-reversible surface-confined process when $k^{0\prime} = 50$ s^{-1} and $\alpha = 0.5$ and when charging current is present. The parameters used in the simulation are similar to those that will be encountered in studies on azurin and reveal that a significant charging current component is associated with the dc and all odd harmonic components. Charging current does not affect the intensity of the even harmonic power spectra, but it does contribute to the dc and odd harmonic components of the power spectra. Thus, under practical conditions, there is no significant advantage in analyzing the odd harmonic components of a ramped square-wave voltammogram, as the Faradaic-to-charging current ratio is not too dissimilar from that found in linear scan dc voltammetry. Furthermore, the Faradaic-to-charging current ratio cannot be improved simply by increasing the surface concentration of the metalloprotein, as data in Figure 5 and those obtained experimentally already refer to conditions that equate to approximately a monolayer coverage.

3.4.1.2. Second Harmonic Component. 3.4.1.2.1. Dependence on $k^{0\prime}$. Ideally, neither the charging process nor a reversible Faradaic process give rise to any even harmonic components. However, a quasi-reversible process is predicted to exhibit even harmonic Faradaic components[29] as evidenced by the finite response for all even harmonics in the power spectrum (Figure 5a). For the purpose of establishing the existence of this ideal combination of zero charging current but finite current for a quasi-reversible surface-confined process, simulated data obtained with a square-wave perturbation described by eq 6 are considered in detail.

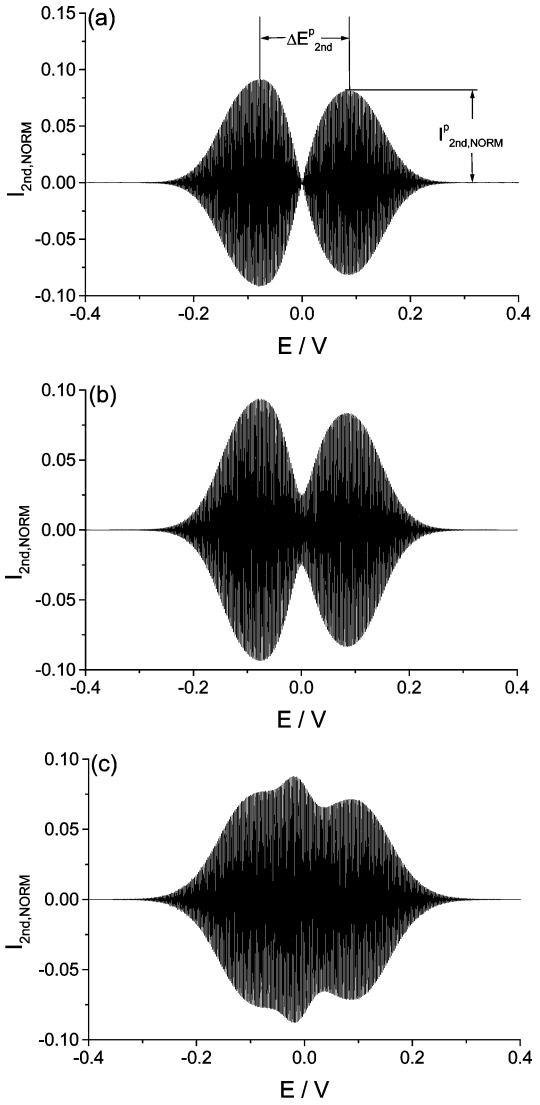

Figure 6. Normalized second harmonic component of quasi-reversible voltammograms simulated using the parameters $k^{0\prime} = 2$ s^{-1}, $v = 50$ mV s^{-1}, $f = 10$ Hz, $E^{0\prime} = 0$, $\Delta E = 50$ mV, $\alpha = 0.5$, and $C_{dl} = 0$. Part (a) represents the response for a superimposed square wave (defined by eq 6) and also defines the terms $I^{p}_{second,NORM}$ and ΔE^{p}_{second}. The result obtained with $C_{dl} = 0.2$ F m^{-2} is essentially identical. In (b) and (c), the waveform is defined by eq 7 and $K = 2$ (b) and 1 (c).

As shown in Figure 6a, for a quasi-reversible case, even with a slow rate constant $k^{0\prime} = 2$ s^{-1} and $\alpha = 0.5$, a well-defined second harmonic voltammetric response is still detected, which is unaltered when a value of $C_{dl} = 0.2$ F m^{-2} is included in the simulations.

The square-wave response is significantly different from that obtained when a two-sine-wave combination (Figure 6b) or a single sine wave (Figure 6c) is applied (on the basis of use of eq 7 with the same parameters as those used to obtain Figure 6a). Remarkably, the second harmonic is absent for a fully reversible process (large $k^{0\prime}$ value), but the magnitude of the

TABLE 1: Dependence of ΔE^{p}_{second} and $I^{p}_{second,NORM}$ on $k^{0'}$ for the Second Harmonic Component of a Quasi-Reversible Square-Wave Voltammogram[a]

$k^{0'}$ (s^{-1})	ΔE^{p}_{second} (mV)	$I^{p}_{second,NORM}$ at positive potential
1000	76	0.220
500	76	0.459
200	76	1.12
150	76	1.44
100	76	1.97
50	76	2.77
40	80	2.86
30	82	2.78
20	85	2.37
10	100	1.18
8	109	0.873
5	129	0.421
2	174	0.0816
1	189	0.0215
0.1	250	0.00300

[a] Simulated with $\upsilon = 50$ mV s^{-1}, $f = 10$ Hz, $\Delta E = 50$ mV, $\alpha = 0.5$, and other parameters as reported in the text.

response initially increases with a decrease of $k^{0'}$ and then decreases until only a very small second harmonic response is detected when the electron-transfer reaction approaches the irreversible case (small $k^{0'}$ value). That is, the peak height, $I^{p}_{second,NORM}$, and peak separation, ΔE^{p}_{second}, (exemplified in Figure 6a) of the second harmonic square-wave voltammograms are highly sensitive to the kinetics of a quasi-reversible process. Details of the dependence of $I^{p}_{second,NORM}$ on $k^{0'}$ (increases, reaches a maximum value, and then decreases) can be ascertained by the inspection of data contained in Table 1. In contrast, ΔE^{p}_{second}always increases as $k^{0'}$ decreases (Table 1). The envelope shape is a function of both α (see next section) and $k^{0'}$.

3.4.1.2.2. Dependence on α. Square-wave voltammetric second harmonic components are highly sensitive to the value of α for a quasi-reversible process, provided there is a significant departure from reversibility (Figure 7). Therefore, if $k^{0'}$ is known, the α value may be determined from the peak current ratio of the two lobes, $I^{p}_{second,NORM}/I^{p1}_{second,NORM}$ (see Figures 6 and 7 for examples). The sensitivity to α is far greater than in the case with dc voltammograms. Analogous dependences on α also are observed in the second harmonic component in sinusoidal ac voltammetry,[13] although the two lobes are better resolved under square-wave conditions.

3.4.1.2.3. Dependence of $I^{p}_{second,NORM}$ on ΔE and f. Data in Figure 8 calculated from simulated quasi-reversible processes with three $k^{0'}$ values show that $I^{p}_{second,NORM}$ exhibits a strong dependence on ΔE values in the range of 0 to 100 mV. For large amplitudes, $I^{p}_{second,NORM}$ becomes independent of ΔE, as also is the case with the odd harmonics, when a process involving solution-soluble species is considered.[8]

$I^{p}_{second,NORM}$ also increases when f increases, reaches a maximum value, and then decreases at high values of f as shown in the data in Table 2 for the case of $k^{0'} = 50$ s^{-1}. Analogous results were obtained when $k^{0'} = 10$ or 100 s^{-1}.

3.4.1.3. Other Even Harmonic Components. The simulated power spectra presented in Figures 9 and 10 clearly show that all even harmonic square-wave components depend significantly on $k^{0'}$ (the time scale of the electron-transfer process), f (time scale of ac measurement), and ΔE, and each may provide a method of estimation of the electron-transfer rate. However, in a phenomenological sense, the characteristics of the higher even harmonic components mimic the second, and need not be discussed in any detail.[30]

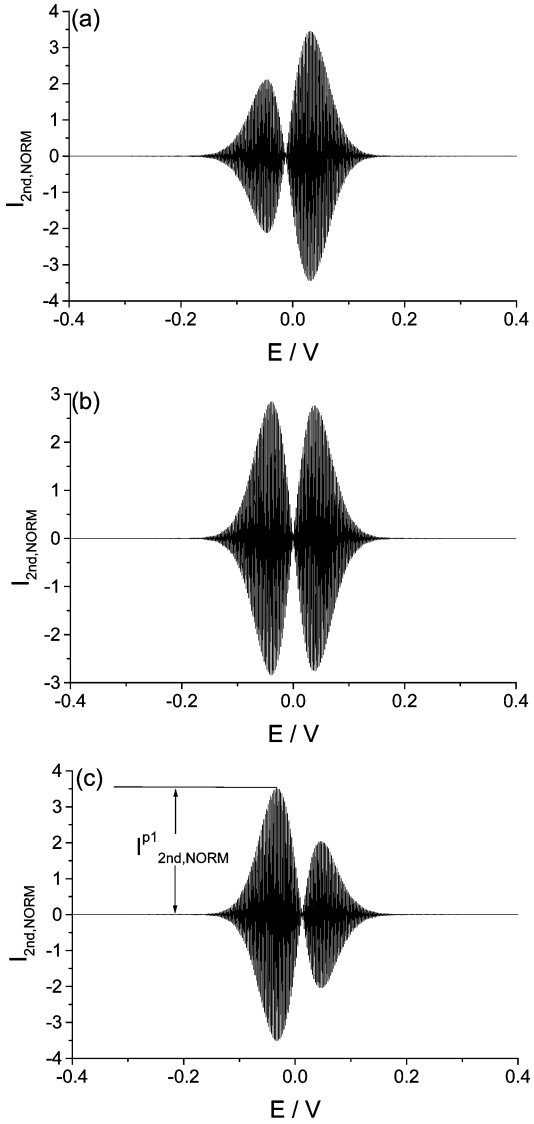

Figure 7. Dependence of the second harmonic component of quasi-reversible square-wave voltammograms on α simulated with parameters defined in the text and $k^{0'} = 50$ s^{-1}, $f = 10$ Hz, $E^{0'} = 0$, $\Delta E = 50$ mV, $\upsilon = 50$ mV s^{-1}, and $\alpha = 0.4$ (a), 0.5 (b), and 0.6, and also defined $I^{p1}_{second,NORM}$ (c).

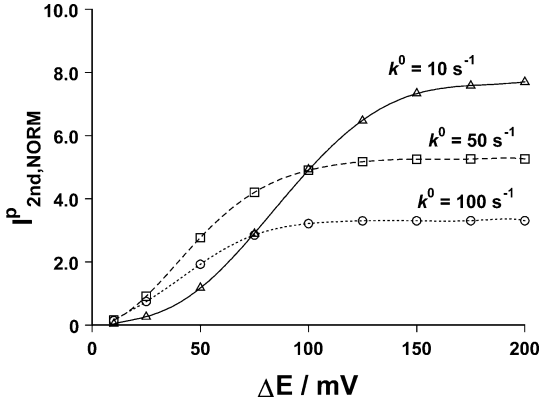

Figure 8. Dependence of $I^{p}_{second,NORM}$ on ΔE for the second harmonic component of quasi-reversible square-wave voltammogram simulated with $f = 10$ Hz, $\alpha = 0.5$, $\upsilon = 50$ mV s^{-1}, and other parameters defined in the text, and $k^{0'} = 10$ (△), 50 (□), and 100 (○) s^{-1}.

3.4.2. Conditions Required for Achieving Equivalence of Approaches Based on Eqs 6 and 7. Even though it is numerically efficient to generate a square wave using eq 6, as noted already,

TABLE 2: Dependence of $I^{p}_{second,NORM}$ on f for a Quasi-Reversible Surface-Confined Process[a]

	$I^{p}_{second,NORM}$		
f/Hz	$\Delta E = 25$ mV	$\Delta E = 50$ mV	$\Delta E = 100$ mV
2	0.0677	0.182	0.282
4	0.242	0.666	1.05
6	0.463	1.33	2.20
8	0.699	2.05	3.48
10	0.915	2.77	4.90
15	1.252	4.21	8.73
20	1.52	5.30	12.2
25	1.55	5.90	15.4
30	1.54	6.13	18.1
35	1.52	6.30	20.2
40	1.51	6.34	22.1
50	1.36	6.03	25.0
60	1.25	5.72	26.7
70	1.14	5.22	27.7
80	1.06	4.86	28.2
100	0.884	4.31	27.8

[a] Simulated with $\upsilon = 50$ mV s^{-1}, $\alpha = 0.5$, $k^{0\prime} = 50$ s^{-1}, and other parameters defined in the text.

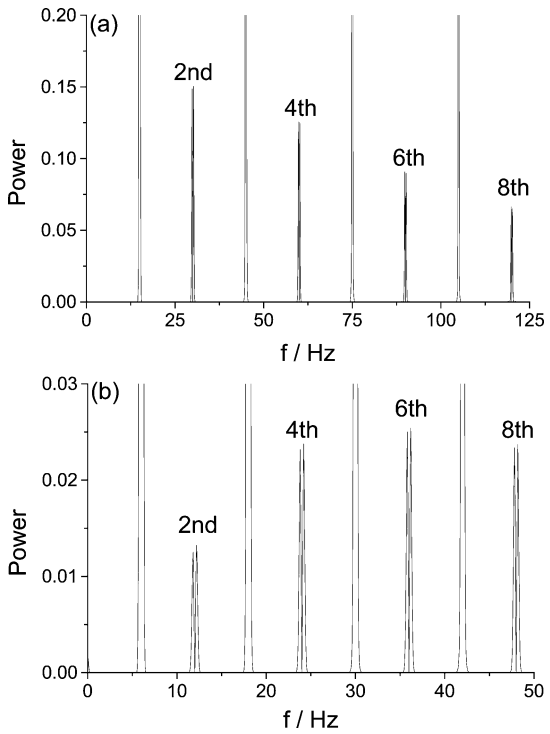

Figure 9. Effect of the frequency (a, 15 Hz; b, 6 Hz) of the square wave on the even harmonic power distribution. The results were simulated with $k^{0\prime} = 50$ s^{-1}, $\upsilon = 50$ mV s^{-1}, $\alpha = 0.5$, $C_{dl} = 0$, and $\Delta E = 50$ mV. The numeral attached to each curve represents the number of the even harmonic component.

it is experimentally convenient to approximate a square wave via the summation of a finite series of sine waves. This is because the discontinuities in the applied signal, even if they could be generated, would evoke infinite responses. Consequently, theoretical analysis of the surface-confined process was undertaken to establish conditions under which a multisine-wave voltammogram (potential modulation described by eq 7) is experimentally indistinguishable to that of the square-wave voltammogram (potential modulation described by eq 6). Obviously, when $K \rightarrow \infty$, eqs 6 and 7 are indistinguishable. The results of theoretical analysis (Table 3) of the second harmonic component reveal that the second harmonic voltammograms obtained when more than 20 sine-wave terms are employed are likely to be experimentally indistinguishable from that predicted for a true square wave if $k^{0\prime} < 200$ s^{-1}. If $k^{0\prime} > 200$ s^{-1}, additional sine-wave terms are needed to achieve this equivalence, or alternatively, a higher scan rate could be used (effectively reducing the reversibility of the electrode reaction according to the relationship in the notes[28c]) to achieve this equivalence. Significantly, the results in Table 3 reveal that the dependence of $I^{p}_{second,NORM}$ on the number of sine-wave terms can be used to provide information on $k^{0\prime}$. For example, the ratio of the second harmonic peak current obtained with a single sine-wave term (eq 7 with $K = 1$) and a perfect square-wave voltammogram enables $k^{0\prime}$ to be measured without knowing the surface concentration of the redox active species.

Theoretical studies with square-wave amplitudes of 25 and 100 mV and at a scan rate of 50 mV s^{-1} in conjunction with data presented in Table 3 lead to the conclusion that the ratio of the second harmonic peak current of single sine-wave and square-wave voltammograms is enhanced when ΔE increases, but this ratio is relatively insensitive to the scan rate when $k^{0\prime} > 10$ s^{-1}.

The close equivalence achieved by using 20 sine-wave terms (eq 7) or a square wave (eq 6) is confirmed by noting that the power spectra (first through tenth) for a quasi-reversible process (double layer charging is omitted to emphasize the Faradaic process) differ by $\leq 1\%$ under the conditions of Figure 11 and confirm the suitability of using eq 7 to generate a good approximation of a square-wave voltammetry without introducing any discontinuity.

4. Experimental Studies with Azurin

Experimental studies to probe the practical usefulness of square-wave voltammetry in the quantitative evaluation of a surface-confined process were undertaken with azurin at a PIGE electrode. This metalloprotein undergoes a Cu(II) to Cu(I) surface-confined process of the kind[2a,7a,12−14]

$$\mathrm{Az[Cu(II)]_{surface}} + \mathrm{e^-} \rightleftarrows \mathrm{Az[Cu(I)]_{surface}} \qquad (32)$$

Previous studies[13] showed this to be a quasi-reversible process, and on this basis, it should be ideal to demonstrate the predicted advantages of even harmonic measurements in Fourier transformed square-wave voltammetry. We describe a strategy that enables each of the unknown parameters of C_{dl}, $E^{0\prime}$, $k^{0\prime}$, α, and Γ to be determined and compared with values obtained by dc and sinusoidal techniques.[13,14] Experimental square-wave data were obtained, using the first 20−140 sine-wave terms of the Fourier series (eq 7).

4.1. Dc and Odd Harmonic Components. Dc cyclic voltammograms of azurin, obtained after the separation of this frequency-independent component from all the ac components, via Fourier analysis, exhibit a small Faradaic current superimposed on a dominant background response (data not shown). A C_{dl} value of about 1.3 F m^{-2} is calculated for a conventional dc experimental ($\Delta E = 0$) case at a potential of 0.3 V versus Ag/AgCl (Figure 12a), but clearly, the background current in this and any other experiments is not potential-independent, as assumed in the simulations. After subtraction of the dc background from Fourier transformed dc components, using baseline-correction software that employed a cubic spline,[31] the more clearly detected Faradaic dc oxidation component (Figure 12b) is seen to exhibit the predicted (Figure 3) amplitude-dependent peak splitting. The Γ value of $(5 \pm 2) \times 10^{-11}$ mol cm^{-2} calculated for the surface coverage, based on the peak area of the background-corrected linear sweep voltammogram

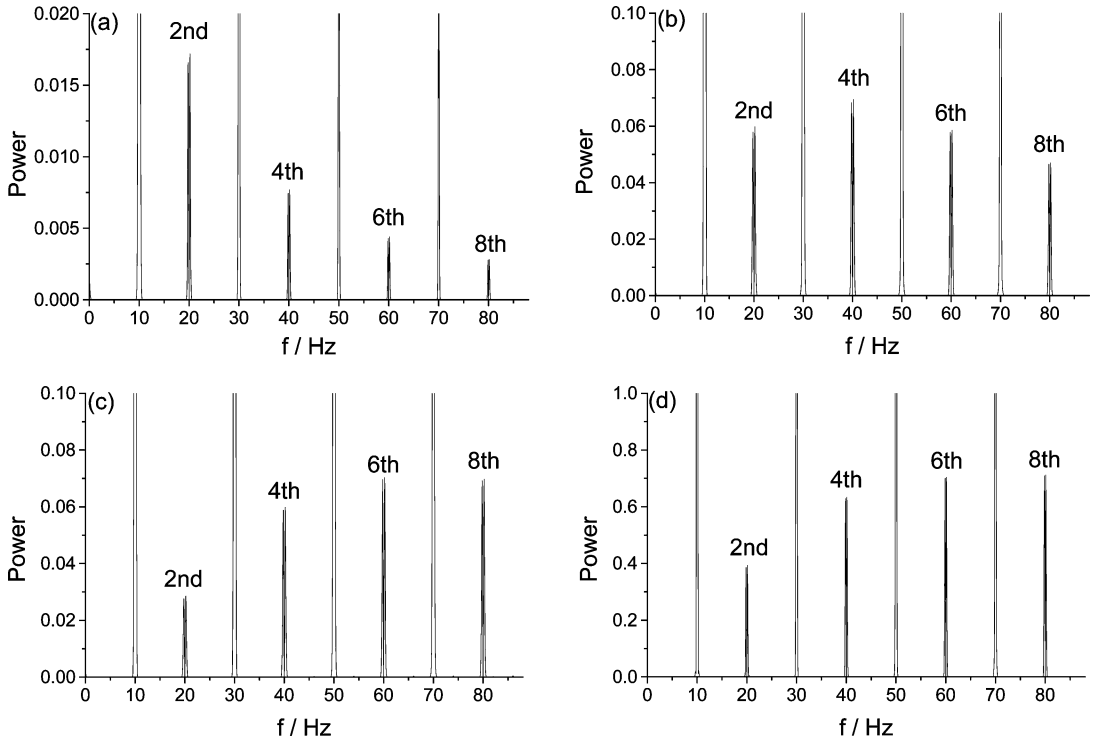

Figure 10. Effect of the $k^{0'}$ (a, 10; b, 50; c, 100 s^{-1}; and $\Delta E = 50$ mV) and ΔE (d, 100 mV and $k^{0'} = 50$ s^{-1}) of the square wave on the even harmonic power distribution. The results were simulated with $f = 10$ Hz, $\upsilon = 50$ mV s^{-1}, $\alpha = 0.5$, and $C_{dl} = 0$. The numeral attached to each curve represents the number of the even harmonic component.

TABLE 3: Dependence of $I^{p}_{Second,NORM}$ on $k^{0'}$ and the Number of Sine-Wave Terms (K) Applied[a]

	$k^{0'}$/ s^{-1}								
K	reversible	1000	500	200	150	100	50	10	1
1	6.51	6.49	6.46	6.32	6.20	5.88	4.83	1.13	*b*
3	1.59	1.59	1.63	1.84	1.99	2.27	2.78	1.19	0.0219
5	0.938	0.954	1.02	1.37	1.60	2.02	2.78	1.19	0.0217
7	0.669	0.696	0.786	1.23	1.50	1.98	2.78	1.19	0.0216
10	0.469	0.510	0.630	1.15	1.45	1.98	2.78	1.19	0.0215
20	0.235	0.317	0.493	1.12	1.45	1.98	2.78	1.18	0.0215
40	0.118	0.248	0.463	1.12	1.45	1.98	2.78	1.18	0.0215
60	0.0785	0.235	0.462	1.12	1.45	1.97	2.77	1.18	0.0215
80	0.0589	0.231	0.462	1.12	1.45	1.97	2.77	1.18	0.0215
100	0.0471	0.229	0.462	1.12	1.45	1.97	2.77	1.18	0.0215
200	0.0248	0.226	0.461	1.11	1.45	1.97	2.77	1.18	0.0215
square wave[c]	*d*	0.220	0.459	1.11	1.44	1.97	2.77	1.18	0.0215

[a] $\alpha = 0.5$, $f = 10$ Hz, $\Delta E = 50$ mV, and $\upsilon = 50$ mV s^{-1}. [b] $I^{p}_{second,NORM}$ cannot be measured. Almost no separation exists between two lobes of the second harmonic voltammogram, so $I^{p}_{second,NORM}$ cannot be measured. [c] Generated using eq 6. [d] $I^{p}_{second,NORM}$ is negligible for a reversible process when a square wave is generated by eq 6.

obtained when $\Delta E = 0$, is consistent with that of $(4 \pm 2) \times 10^{-11}$ mol cm^{-2} reported in previous studies.[13]

The average of the peak potentials obtained from the split waves obtained at large amplitudes (Figure 12b), the potential at the minimum current between these two peaks (Figure 12b) for ΔE up to 175 mV, and the average of the peak potential obtained from cyclic voltammogram (Figure 12a) all have values of (25 ± 5) mV versus Ag/AgCl. These values may be compared to the $E^{0'}$ value of 220 mV versus standard hydrogen electrode (SHE) (or 23 mV versus Ag/AgCl[6]) obtained in dc cyclic voltammetric studies under similar conditions.[14] A peak potential of 20 ± 5 mV versus Ag/AgCl obtained by averaging the reduction and oxidation components is in good agreement with the reversible potential deduced from the dc cyclic voltammogram. Thus, the dc component of the square-wave voltammogram may be regarded as close to reversible under the conditions used to obtain voltammograms presented in Figure 12. However, the unfavorable Faradaic-to-background current ratio presents considerable difficulty in undertaking a quantitative evaluation of the electrode kinetics.

As predicted theoretically (Figure 5c), the first (Figure 13) and all other odd harmonics of Fourier transformed square-wave voltammograms obtained from surface-bound azurin also are dominated by the background current. A C_{dl} value of 1.0 F m^{-2} is estimated from the first harmonic component, at a potential of 0.3 V, which agrees well with the value of 1.3 F m^{-2} obtained from the dc voltammogram.

4.2. Second Harmonic Component. *4.2.1. Evaluation of* $k^{0'}$, α, *and* Γ. The observation of a significant second harmonic component (Figure 14) immediately confirms that the azurin system is a quasi-reversible rather than reversible process. Additionally, and as theoretically predicted, the background current that dominates the dc and odd harmonic ac components is now negligible relative to the Faradaic current. Consequently, in the second (Figure 14) and higher even harmonic components,

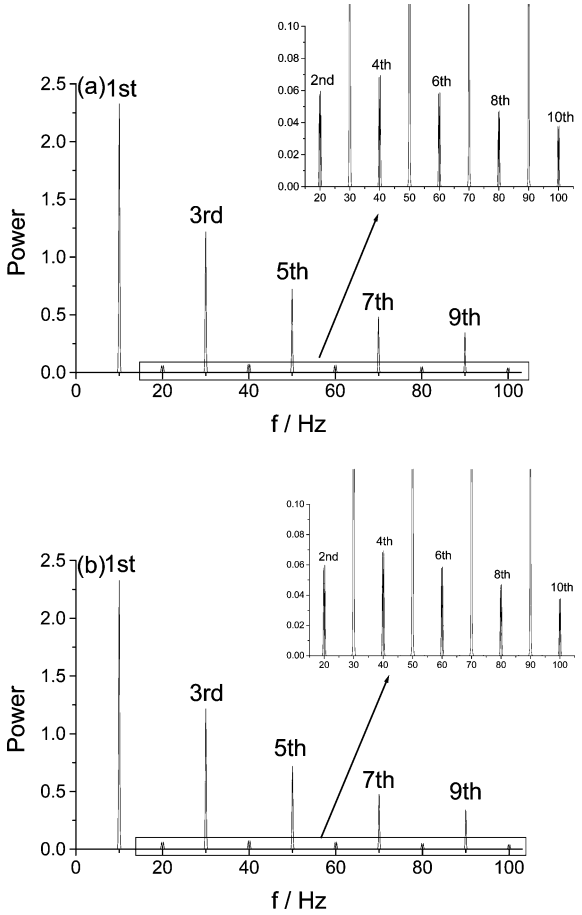

Figure 11. Power spectra of the square wave (generated using (a) 20 sine waves (eq 7) and (b) square wave (eq 6)) voltammograms simulated using the following parameters: $f = 10$ Hz, $\upsilon = 50$ mV s^{-1}, $k^{0\prime} = 50$ s^{-1}, $\alpha = 0.5$, and $C_{dl} = 0$. The number attached to each curve is the number of the even harmonic component.

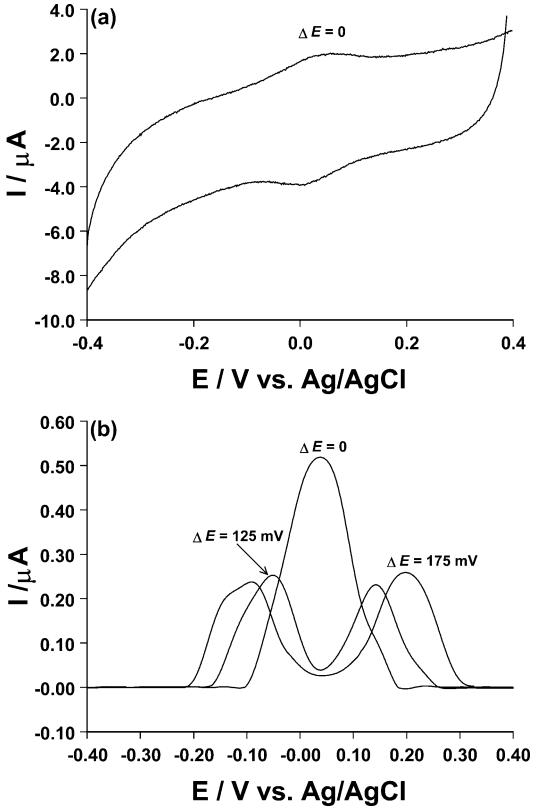

Figure 12. A cyclic ($\Delta E = 0$) dc voltammogram (a) and the dc components of Fourier transformed square-wave (b) voltammograms obtained from azurin immobilized on a PIGE before (a) and after (b, oxidation component only shown) background subtraction. $\upsilon = 50$ mV s^{-1}, $f = 9.54$ Hz, and number of sine-wave term = 70.

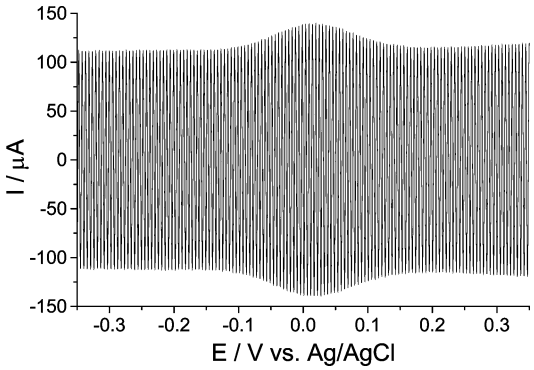

Figure 13. First harmonic component derived from a Fourier transformed square-wave voltammogram of surface-confined azurin: $\upsilon = 50$ mV s^{-1}, $f = 9.54$ s^{-1}, $\Delta E = 50$ mV, and number of sine-wave terms = 70.

the need for an arbitrary background correction as a precursor to analysis of the Faradaic current component is therefore eliminated.

There are numerous approaches available to estimate $k^{0\prime}$ and α from the second harmonic component. A method we advocate that has the advantage of avoiding the need to assume a value of Γ (and $E^{0\prime}$) is to measure the ratio of the square-wave second harmonic peak current relative to that obtained when only the first term in the Fourier series is used and compare this value with the simulated ratios. In the first instance, an α value of 0.5 is assumed, noting that the fact that the two lobes of the second harmonic are close to symmetrical is consistent with this estimation. Once $k^{0\prime}$ is calculated, a more precise value of α can be estimated from the peak current ratio of the two second harmonic square-wave lobes. By iterative application of this two-step protocol, a $k^{0\prime}$ value of 90 ± 10 s^{-1} and an α value of 0.48 ± 0.02 were obtained. The $k^{0\prime}$ value may be compared to the value of 70 ± 10 s^{-1} deduced from the dependence of the peak separation on the scan rate from background-corrected dc cyclic voltammograms.[13] The dc technique is very insensitive to α.

I^{p}_{second} values obtained over a wide range of conditions (Table 4) agree well with theoretical values predicted on the basis of $\Gamma = (4 \pm 2) \times 10^{-11}$ mol cm^{-2} using $k^{0\prime} = 90$ s^{-1} and $\alpha = 0.48$. This value agrees satisfactorily with $(5 \pm 2) \times 10^{-11}$ mol cm^{-2} deduced from the dc voltammetric studies (see preceding sections), $(4 \pm 2) \times 10^{-11}$ mol cm^{-2} reported[13] under conditions of dc cyclic voltammetry, and $(3 \pm 1) \times 10^{-11}$ mol cm^{-2} obtained from second harmonic sinusoidal voltammetry.[13]

Data describing the effect of ΔE and f on I^{p}_{second} are summarized in Figure 15 and Table 5. As theoretically predicted (Figure 8), I^{p}_{second} increases rapidly for ΔE values of <100 mV, then more slowly until I^{p}_{second} becomes almost independent of ΔE when $\Delta E >$ 150 mV. The magnitude of I^{p}_{second} also increases as f increases (2.38 to 38.15 Hz) as predicted by simulation (Table 2).

4.2.2. Detection of Nonideality. The $k^{0\prime}$ and α values, as deduced already, are obtained from potentials close to the reversible value, rather than over the entire potential range where significant Faradaic current is detected. Figure 16 shows the full simulation of dc and ac components of the square-wave

TABLE 4: Dependence of Square-Wave Second Harmonic Peak Current, I^{p}_{second}, on the Number of Sine-Wave Terms, *K*, Employed (eq 6) to Generate Square-Wave Voltammograms of Surface-Confined Azurin at a PIGE Electrode[a]

	I^{p}_{second} at positive potential (μA)					
	$\upsilon = 50$ mV s^{-1}			$\upsilon = 100$ mV s^{-1}		
K	$\Delta E = 25$ mV	$\Delta E = 50$ mV	$\Delta E = 100$ mV	$\Delta E = 25$ mV	$\Delta E = 50$ mV	$\Delta E = 100$ mV
1	3.05	10.1	20.3	3.00	9.92	21.1
3	1.31	4.22	9.02	1.19	3.90	8.11
5	1.26	4.03	7.15	1.14	3.45	7.45
7	1.22	3.67	6.20	1.11	3.34	6.27
10	1.20	3.60	5.88	1.06	3.26	5.74
20	1.17	3.57	5.82	1.10	3.20	5.67
30	1.20	3.61	5.86	1.09	3.22	5.61
40	1.23	3.55	5.85	1.07	3.18	5.63
50	1.21	3.59	5.82	1.11	3.22	5.66
60	1.18	3.57	5.85	1.06	3.16	5.60
70	1.20	3.60	5.81	1.08	3.19	5.57
80				1.07	3.21	5.61
100				1.09	3.25	5.59
120				1.06	3.20	5.63
140				1.07	3.22	5.61

[a] Values are for one particular data set. Variation between each experiment is governed by $\Gamma = (4 \pm 2) \times 10^{-11}$ mol cm^{-2}.

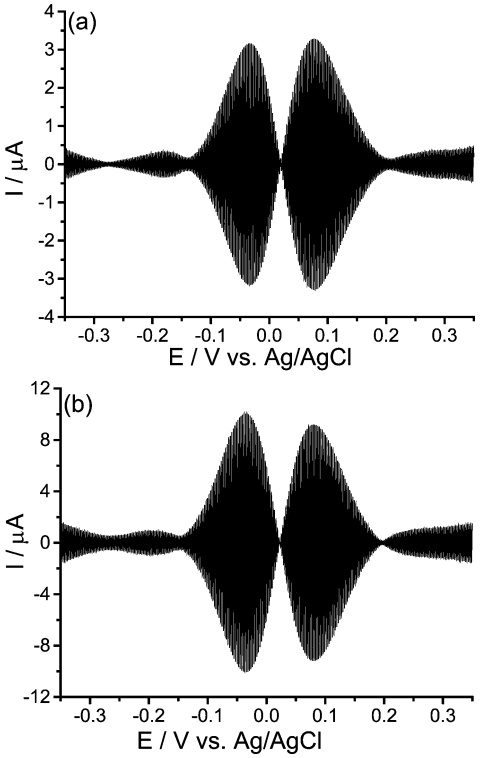

Figure 14. Second harmonic components of Fourier transformed square-wave voltammograms obtained for surface-confined azurin obtained at a PIGE electrode when $\upsilon = 50$ mV s^{-1}, $f = 9.54$ Hz, and $\Delta E = 50$ mV. (a) Square-wave voltammogram based on the first 70 terms in eq 6. (b) Sinusoidal voltammogram obtained using the first term in eq 6.

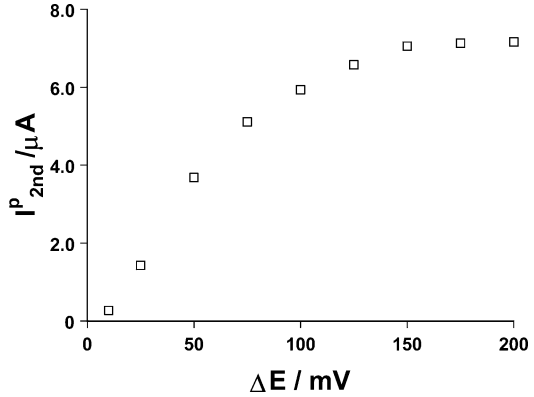

Figure 15. Dependence of I^{p}_{second} on ΔE obtained from Fourier transformed square-wave voltammogram of azurin. $\upsilon = 50$ mV s^{-1}, $f = 9.54$ Hz, and $K = 53$.

TABLE 5: Dependence of the Second Harmonic Peak Current (at positive potential) on Frequency Obtained from Fourier Transformed Square-Wave Voltammetry of Surface-Confined Azurin[a]

	I^{p}_{second} (μA)		
f (Hz)	$\Delta E = 25$ mV	$\Delta E = 50$ mV	$\Delta E = 100$ mV
2.38	0.075	0.199	0.433
4.77	0.311	0.845	1.28
9.54	1.08	2.83	4.69
19.07	2.93	8.14	13.97
38.15	4.19	14.93	33.89

[a] $\upsilon = 50$ mV s^{-1}.

voltammogram obtained using the parameters deduced from the analysis of peak current data: $\Gamma = 3 \times 10^{-11}$ mol cm^{-2}; $E^{0'} = 25$ mV; $k^{0'} = 90$ s^{-1}; $\alpha = 0.48$; $A = 0.2827$ cm^2; $T = 273$ K; $C_{dl} = 1.0$ F m^{-2}; and other conditions stated in the caption to the figure. A comparison of experimental and simulated (Figure 16) data in the global context reveals that the peak-to-peak separation of 119 mV obtained in the second harmonic lobes (Figure 14b) is significantly larger than theoretically predicted for a $k^{0'}$ value of 90 s^{-1} (Table 1, Figure 16d). Peak widths at half-height are also broader than theoretically predicted. The broader than theoretically expected wave shapes also reported in sine-wave[13] and dc voltammetric studies on azurin[2a,7a,12] and for other surface-confined processes[2a,4] have been attributed to kinetic and/or thermodynamic dispersion,[32] hysteresis produced by the shape of the reaction coordinate,[33] and other causes.[34]

Some aspect of the nonideality exhibited in the power spectrum obtained from Fourier transformed square-wave voltammograms with surface-bound azurin are consistent with frequency dispersion. Thus, the relative magnitudes of the second, fourth, sixth, and eighth even harmonic components are not fully consistent with a single $k^{0'}$ value for all azurin molecules of 90 s^{-1} (compare theoretically predicted (Figure 16a) and experimentally found (Figure 17) trends). The uncompensated resistance of ca. 30 Ω has only a very small influence on the power spectrum detected experimentally. Analogously, in sinusoidal ac voltammetry,[13] the third harmonic

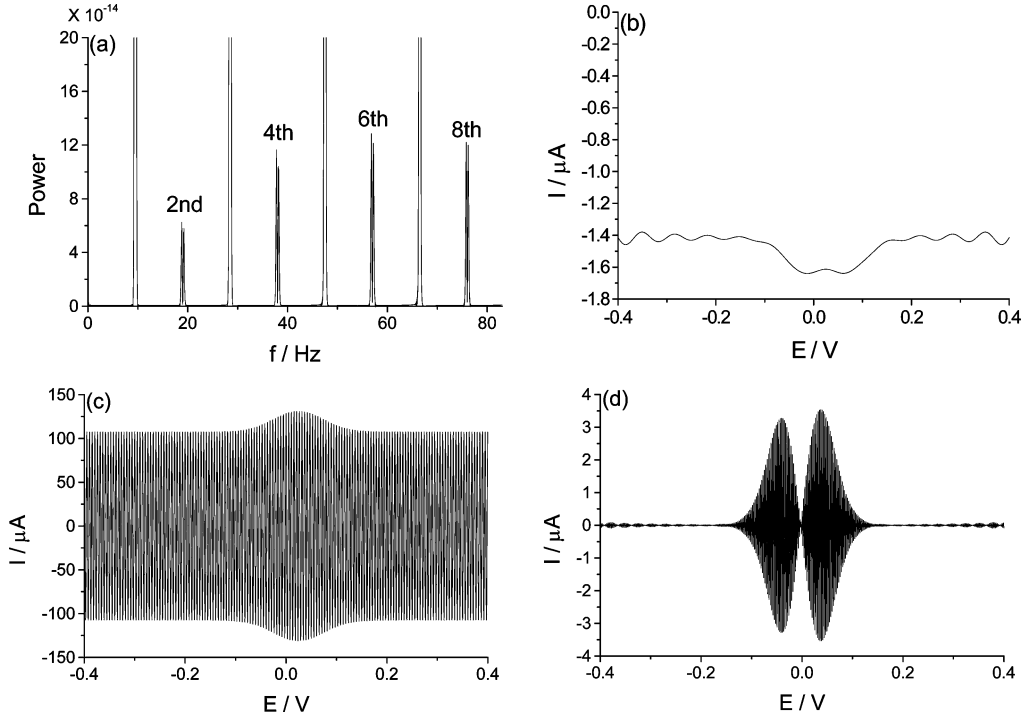

Figure 16. Simulated Fourier transformed voltammetry obtained using $\upsilon = 50$ mV s^{-1}, $f = 9.54$ Hz, $\Delta E = 50$ mV, number of sine-wave terms = 70, and other parameters defined in the text.

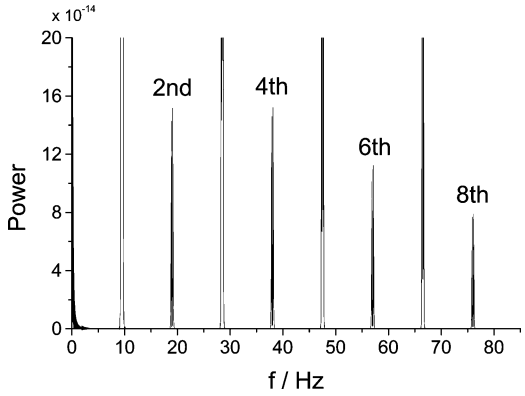

Figure 17. Power spectrum obtained from Fourier transformed square-wave voltammetry of surface-bound azurin. Experimental conditions are the same as for Figure 14a.

current is smaller than theoretically predicted on the basis of $k^{0\prime}$ value predicted from the analysis of lower-order harmonics and dc terms. That is, if randomly oriented adsorbed azurin molecules exhibit a range of $k^{0\prime}$ values rather than a single $k^{0\prime}$ value partially due to the variation of the distance between the redox center and electrode surface, then a shorter time scale (higher harmonic components) will discriminate against the more irreversible processes and give lower current magnitudes than expected on the basis of the assumption that all molecules exhibit the same $k^{0\prime}$ value, as deduced from data obtained at lower frequencies or longer time scales. Thermodynamics dispersion (variability of $E^{0\prime}$) also could contribute to wave broadening.

5. Conclusions

A theoretical analysis of the technique of Fourier transformed ramped square-wave voltammetry of surface-bound species leads to the prediction of an unusual form of both kinetic and background current selectivity in the even harmonic components. Thus, no even harmonics response is predicted for a reversible process. In contrast, a finite response is predicted for a quasi-reversible process. At the same time, the background charging current is predicted to be absent for the even harmonics so that an extremely favorable Faradaic-to-charging current ratio is available for the analysis of quasi-reversible processes when second or other even harmonic data are used. Theoretical studies also establish conditions where the use of a multisine-wave approach provides voltammograms that are experimentally indistinguishable from those expected for a true ramped square wave and demonstrate that the use of the ratio of the peak current of the second harmonic component for ac voltammograms obtained under square-wave and sinusoidal-wave conditions provides a simple and sensitive method for the calculation of $k^{0\prime}$. The even harmonics also provide a very sensitive method for the estimation of α. An analogous situation prevails when O and R in eq 1 are soluble.[35]

Experimental studies on the reduction of surface-bound azurin at a PIGE electrode confirm most of the theoretical predictions. The value of $k^{0\prime} = 90 \pm 10$ s^{-1} deduced on the basis of second harmonic peak current magnitudes is in good agreement with data obtained by background-corrected dc cyclic voltammograms. Nonideality detected in square-wave voltammograms is consistent with kinetic dispersion. The ability to measure the second and other even harmonics in the virtual absence of any charging current provides a significant advantage of Fourier transformed square-wave voltammetry.

Acknowledgment. The authors gratefully acknowledge the Australian Research Council, the Monash University Research Fund, and the Natural Sciences and Engineering Research Council of Canada for financial support of this project. We also thank Prof. Fraser Armstrong and Dr. H. A. Heering (Inorganic Chemistry Laboratory, Oxford University, U.K.) for provision of the software used for baseline subtraction and Dr. A. DiBilio for the provision of high-purity *P. aeruginosa* azurin. M.J.H. would like to dedicate this paper to Steve Waugh on the occasion of his retirement.

References and Notes

(1) Finklea, H. In *Electroanalytical Chemistry*; Bard, A. J., Rubinstein, I., Eds.; Marcel Dekker: New York, 1999; Vol. 19, p 110.

(2) (a) Armstrong, F. A.; Heering, H. A.; Hirst, J. *Chem. Soc. Rev.* **1997**, *26*, 169. (b) Armstrong, F. A.; Wilson, G. S. *Electrochim. Acta* **2000**, *45*, 2623.

(3) Kuznetsov, A. M.; Ulstrup, J. *Electrochim. Acta* **2000**, *45*, 2339.

(4) Bond, A. M. *Broadening electrochemical horizons: principles and illustration of voltammetric and related techniques*; Oxford University Press: Oxford, 2002.

(5) Laviron, E. In *Electroanalytical Chemistry*; Bard, A. J., Ed.; Marcel Dekker: New York, 1982; Vol. 12, p 53.

(6) Bard, A. J.; Faulkner, L. R. *Electrochemical Methods: Fundamentals and Applications*, 2nd ed.; John Wiley & Sons: New York, 2001.

(7) (a) Jeuken, L. J. C.; McEvoy, J. P.; Armstrong, F. A. *J. Phys. Chem. B* **2002**, *106*, 2304. (b) O'Connor, S. D.; Olsen, G. T.; Creager, S. E. *J. Electroanal. Chem.* **1999,** *466*, 197. (c) Komorsky-Lovrić, Š.; Lovrić, M. *Electrochim. Acta* **1995**, *40*, 1781. (d) Komorsky-Lovrić, Š.; Lovrić, M. *J. Electroanal. Chem.* **1995**, *384*, 115. (e) Komorsky-Lovrić, Š.; Lovrić, M. *Anal. Chim. Acta* **1995**, *305*, 248. (f) O'Dea, J. J.; Osteryoung, J. G. *Anal. Chem.* **1993**, *65*, 3090. (g) Reeves, J. H.; Song, S.; Bowden, E. F. *Anal. Chem.* **1993**, *65*, 683.

(8) Gavaghan, D. J.; Elton, D. M.; Oldham, K. B.; Bond, A. M. *J. Electroanal. Chem.* **2001**, *512*, 1.

(9) Gavaghan, D. J.; Elton, D. M.; Bond, A. M. *J. Electroanal. Chem.* **2001**, *513*, 73.

(10) Barker, G. C.; Jenkins, J. L. *Analyst* **1952**, *77*, 685.

(11) Osteryoung, J.; O'Dea, J. J. In *Electroanalytical Chemistry*; Bard, A. J., Ed.; Marcel Dekker: New York, 1986; Vol. 14, p 209.

(12) (a) Armstrong, F. A. *J. Chem. Soc., Dalton Trans.* **2002**, 661. (b) Jeuken, L. J. C.; Wisson, L.-J.; Armstrong, F. A. *Inorg. Chim. Acta* **2002**, *331*, 216. (c) Jeuken, L. J. C.; Armstrong, F. A. *J. Phys. Chem. B* **2001**, *105*, 5271. (d) Hirst, J.; Armstrong, F. A. *Anal. Chem.* **1998**, *70*, 5062. (e) Armstrong, F. A.; Butt, J. N.; Sucheta, A. *Methods Enzymol.* **1993**, *227*, 479.

(13) Guo, S.-X.; Zhang, J.; Elton, D. M.; Bond, A. M. *Anal. Chem.* **2004**, *76*, 166.

(14) Rooney, M. B.; Honeychurch, M. J.; Selvaraj, F. M.; Blankenship, R. E.; Bond, A. M.; Freeman, H. C. *J. Biol. Inorg. Chem.* **2003**, *8*, 306.

(15) St. Clair, C. S.; Ellis, W. R.; Gray, H. B. *Inorg. Chim. Acta* **1992**, *191*, 149.

(16) Bond, A. M.; Duffy, N. W.; Elton, D. M.; Guo, S.-X.; Zhang, J. *Anal. Chem.* In press.

(17) Spanier, J.; Oldham, K. B. *An Atlas of Functions*; Hemisphere Publishing Corporation: Washington, 1987.

(18) Scholz, F.; Lange, B. *Trends Anal. Chem.* **1992**, *11*, 359.

(19) Dostal, A.; Meyer, B.; Scholz, F.; Shroder, U.; Bond, A. M.; Marken, F.; Shaw, S. J. *J. Phys. Chem.* **1995**, *99*, 2096.

(20) Scholz, F.; Meyer, B. In *Electroanalytical Chemistry*; Bard, A. J., Ed.; Marcel Dekker: New York, 1998; Vol. 20.

(21) Smith, C. P.; White, H. S. *Anal. Chem.* **1992**, *64*, 2398.

(22) Honeychurch, M. J.; Bond, A. M. *J. Electroanal. Chem.* **2002**, *529*, 3.

(23) Marcus, R. A.; Sutin, N. *Biochim. Biophys. Acta* **1985**, *811*, 265.

(24) Chidsey, C. E. D. *Science* **1991**, *251*, 919.

(25) Oldham, K. B.; Gavaghan, D. J.; Bond, A. M. *J. Phys. Chem. B* **2002**, *106*, 152.

(26) Mirščeki, V.; Lovrić, M. *Electroanalysis* **1997**, *9*, 1283.

(27) See for example: (a) Ohtani, M. *Electrochem. Commun.* **1999**, *1*, 488. (b) Heering, H. A.; Mondal, M. S.; Armstrong, F. A. *Anal. Chem.* **1999**, *71*, 174. (c) Tender, L.; Carter, M. T.; Murray, R. W. *Anal. Chem.* **1994**, *66*, 3173. (d) Weber, K.; Creager, S. E. *Anal. Chem.* **1994**, *66*, 3164.

(28) (a) $\Omega = RT\omega/F\nu$. (b) $\tau = F\nu t/RT$. (c) $K^0_{\mathrm{norm}} = RTk^{0'}/F\nu$. (d) $I_{\mathrm{norm}} = RTI/F^2A\nu\Gamma$. (e) $E^{0'}_{\mathrm{norm}} = FE^{0'}/RT$. (f) $E^{\mathrm{norm}}_{\mathrm{dc}} = FE_{\mathrm{dc}}/RT$. (g) $E^{\mathrm{norm}}_{\mathrm{ac}} = (8\Delta\xi/\pi)\sum_{n=1}^{K}\{\sin[(2n-1)\Omega\tau]/(2n-1)\}$. (h) $E^{\mathrm{norm}}_{\mathrm{ac}} = 2(-1)^{\mathrm{Int}(\omega t/\pi)}\Delta\xi$. (i) $E_{\mathrm{norm}} = E^{\mathrm{norm}}_{\mathrm{dc}} + E^{\mathrm{norm}}_{\mathrm{ac}}$. (j) $K_{\mathrm{f}} = K^0_{\mathrm{norm}}\exp[-\alpha(E_{\mathrm{norm}} - E^{0'}_{\mathrm{norm}})]$. (k) $K_{\mathrm{b}} = K^0_{\mathrm{norm}}\exp[(1-\alpha)(E_{\mathrm{norm}} - E^{0'}_{\mathrm{norm}})]$.

(29) Unpublished results show that there are also even harmonic components in the absence of an underlying dc ramp for a quasi-reversible process.

(30) The response of the even harmonic components is very sensitive to the kinetics, and components higher than the second may be advantageous for measurement of fast rate constants.

(31) Press, W. H.; Flannery, B. P.; Teukolsky, S. A.; Vetterling, W. T. *Numerical Recipes in Pascal*; Cambridge University Press: New York, 1989.

(32) Rowe, G. K.; Carter, M. T.; Richardson, J. N.; Murray, R. W. *Langmuir* **1995**, *11*, 1797.

(33) Feldberg, S. W.; Rubinstein, I. *J. Electroanal. Chem.* **1988**, *240*, 1.

(34) (a) Brown, A. P.; Anson, F. C. *Anal. Chem.* **1977**, *49*, 1589. (b) Albery, W. J.; Boutelle, M. G.; Colby, P. J.; Hillman, A. R. *J. Electroanal. Chem.* **1982**, *133*, 135. (c) Gerischer, H.; Scherson, D. A. *J. Electroanal. Chem.* **1985**, *188*, 33. (d) Rowe, G. K.; Creager, S. E. *Langmuir* **1991**, *7*, 2307. (e) Acevedo, D.; Abruña, H. D. *J. Phys. Chem.* **1991**, *95*, 9590. (f) Smith, C. P.; White, H. S. *Anal. Chem.* **1992**, *64*, 2398. (g) Honeychurch, M. J. *Langmuir* **1998**, *14*, 6291.

(35) Sher, A. A.; Bond, A. M.; Gavaghan, D. J.; Gillow, K.; Feldberg, S. W.; Duffy, N. W.; Guo, S.-X.; Zhang, J. *Electroanalysis* In press.